Uncovering Electromechanical Uncoupling in Subclinical Pathogenic Mutation Carriers and Arrhythmogenic Cardiomyopathy Patients

Manon Kloosterman[1,2], Machteld J. Boonstra[1], Feddo P. Kirkels[1], Cornelis H. Slump[2], Peter Loh[1], Peter M. van Dam[1]

[1]Department of cardiology, University Medical Center Utrecht, Utrecht, the Netherlands
[2]University of Twente, Enschede, the Netherlands

Abstract

Arrhythmogenic cardiomyopathy (ACM) is a progressive inherited heart disease. The clinical presentation of ACM is heterogenous and diagnosis remains challenging. Whereas echocardiographic deformation imaging was capable in detecting subtle functional abnormalities in asymptomatic ACM patients, the 12-lead electrocardiogram (ECG) is still not able to detect these subtle electrical changes. As the 12-lead ECG might not be sensitive enough, this study aimed to relate the electrical changes as recorded by body surface potential mapping (BSPM) to the mechanical changes detected by echocardiographic deformation imaging. Per lead, the integral values of all 67 leads were calculated per 5 ms intervals during ventricular depolarization and the lead in which the absolute minimum appeared the most ($\overrightarrow{lead_{min}}$) was identified. The direction of this vector towards a specific heart segment was then compared to the interval between QRS onset and local onset of myocardial shortening, the electromechanical interval (EMI). We observed a relation of $\overrightarrow{lead_{min}}$ pointing towards the basal segment of the right ventricle (RV_{basal}) and an increased EMI in this area suggesting the existence of an electro-mechanical relationship in RV_{basal}. With this study, the first steps towards relating both electrical and mechanical changes in ACM pathogenic mutation carriers is made.

1. Introduction

Arrhythmogenic cardiomyopathy (ACM) is a progressive inherited heart muscle disease with an estimated prevalence of 1:2000 to 1:5000 and is an important cause of sudden cardiac death among young individuals.[1] Several genes have been identified related to the development of ACM, in which the majority of genes encode for desmosomal proteins. Genetic mutations affecting the desmosomes may result in mechanical dysfunction of cardiomyocytes, fibrofatty myocardial replacement, cardiac conduction delay and ventricular arrythmias.[1][2]

The clinical presentation of ACM is heterogenous and diagnosis remains challenging. Especially accurate prediction and risk-stratification of the development of ACM in asymptomatic mutation carriers is beyond capabilities of current diagnostic tests. This is problematic since ventricular arrhythmias and sudden cardiac death might be the first signs of disease progression.[3]

Recently, the added value of echocardiographic deformation imaging in risk-stratification has been demonstrated in pathogenic mutation carriers who did not yet present electrocardiographic (ECG) abnormalities.[4] However, (subtle) electrical abnormalities are likely to precede these structural abnormalities, but the 12-lead ECG might not be sensitive enough to detect these changes.[2][5] Therefore, we aim to investigate whether electrical changes as recorded by 64-electrode body surface potential mapping (BSPM), is able to differentiate ACM patients and subclinical pathogenic mutation carriers from healthy controls and to relate these electrical differences to echocardiographic deformation imaging to investigate electromechanical uncoupling.

2. Methods

2.1. Study population

A total of 35 subjects of which 11 patients with definite ACM (TFC $\geq$ 4), seven patients with borderline ACM (TFC < 4) and 17 asymptomatic family members (TFC = 2) carrying a plakophilin 2 (PKP2) mutation referred for cardiac MRI were included in this study. The control population[1] (n = 25) consisted of athletes and patients clinically referred to undergo cardiac MRI.

[1] Subjects diagnosed with right ventricular outflow tract tachycardia (n=7) patients with non-cardiac chest pain (n=4), athletes (n=4) and marathoners (n=10).[6]

2.2. Body surface potential mapping

Each subject underwent 67-electrode BSPM (Biosemi/ActiView, 2048 Hz) in the outpatient clinic of the UMC Utrecht for five minutes in supine position. Nine unipolar electrodes were placed on the back and 55 on the chest (Figure 1) referenced to Wilson's Central Terminal derived from the limb leads. Subject specific CT/MRI based anatomical models of the heart/torso were created and electrode positions captured by a 3D camera were registered to the torso.

BSPM signals were then loaded into MATLAB (R2019B) for offline processing and analysis. Signals were down sampled to 1000 Hz, baseline corrected using a 2nd order high-pass Butterworth filter (fc = 0.25 Hz), muscle artifacts were removed using a 2nd order low-pass Butterworth filter (fc = 200 Hz) and powerline artifacts were removed using a 50Hz notch filter. All filters were applied using the '*filtfilt'* function to assure zero-phase distortion.

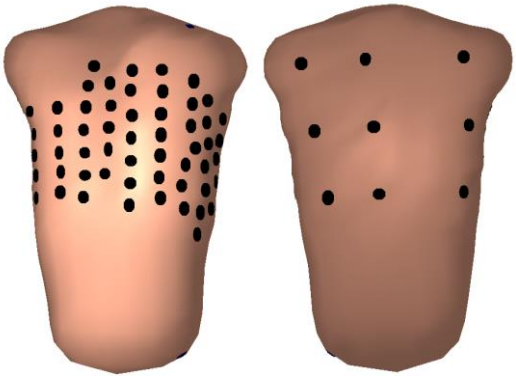

Figure 1: Electrode positions of the 67-electrode BSPM measurement. 64 electrodes are placed on the torso using 12 vertical strips of 28cm with 4cm between adjacent electrodes. Three electrodes are placed on the limbs and used to calculate Wilson's central terminal as a reference for the 64 unipolar leads.

As deformation images are obtained at end expiration, all end-expiratory beats were selected based on local maximal RS amplitude. Therefore, the lead with the highest median RS amplitude was identified, assumed to be the lead in which the effect of respiration was maximal. Per beat, QRS onset and offset was manually annotated using the root mean square (RMS) signal of all leads and beats were baseline corrected so QRS onset was zero. Alignment of beats was optimized my minimizing the relative difference (RD) to the median beat of all end-expiratory beats. Ten beats with the smallest RD to the median beat were then selected and thereof the average end-expiratory beat was determined.

2.3. Echocardiographic deformation imaging

Standard echocardiographic recordings and recordings suitable for deformation imaging were obtained during clinical follow-up of pathogenic mutation carriers (n = 35) and healthy controls (n = 20). To assess right ventricular (RV) function, real-time 2D (B-mode) ultrasound recordings were obtained in the RV-focused apical four chamber view and data was exported for offline 2D speckle tracking analysis. Deformation curves of the apical (RV_{apex}), mid (RV_{mid}) and basal lateral wall (RV_{basal}) of the RV were computed and exported as text files for offline data analysis in MATLAB (R2019B). The electromechanical interval (EMI), defined as the interval between QRS onset and local onset of myocardial shortening, was computed for all segments and classified pathological if EMI > 90ms.[4]

2.4. Data analysis

Per lead, the integral values of the 67 leads were calculated per 5 ms intervals during ventricular depolarization to be able to identify subtle differences. For each interval, the lead with the maximal and minimal integral value was determined. Subsequently, the lead in which the absolute minimum appeared the most ($\overrightarrow{lead_{min}}$) was identified and indicated in each subject specific model using a vector pointing from the center of ventricular mass towards $\overrightarrow{lead_{min}}$. Five regions to which the vector could point were identified: the left ventricle (LV), the right ventricular outflow tract (RVOT) and three segments at the RV free wall; apical-, mid- and basal (Figure 2). Then, $\overrightarrow{lead_{min}}$ was classified to point towards one of these segments to enable comparison of the direction of $\overrightarrow{lead_{min}}$ to the EMI.

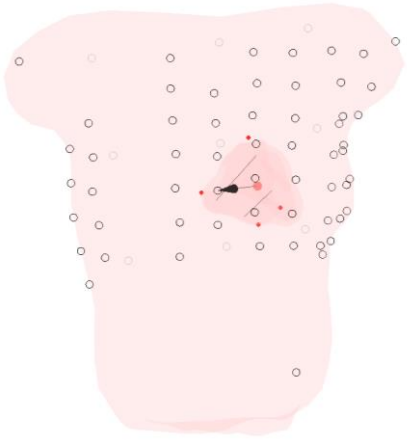

Figure 2: A representative example of a subject specific anatomical model with a vector (black arrow) pointing from the center of ventricular mass (red dot) towards $\overrightarrow{lead_{min}}$. Open dots on the body surface represent placed electrodes, black lines in the RV are representing the division between the three RV free wall segments; RV_{apex}, RV_{mid} and RV_{basal}.

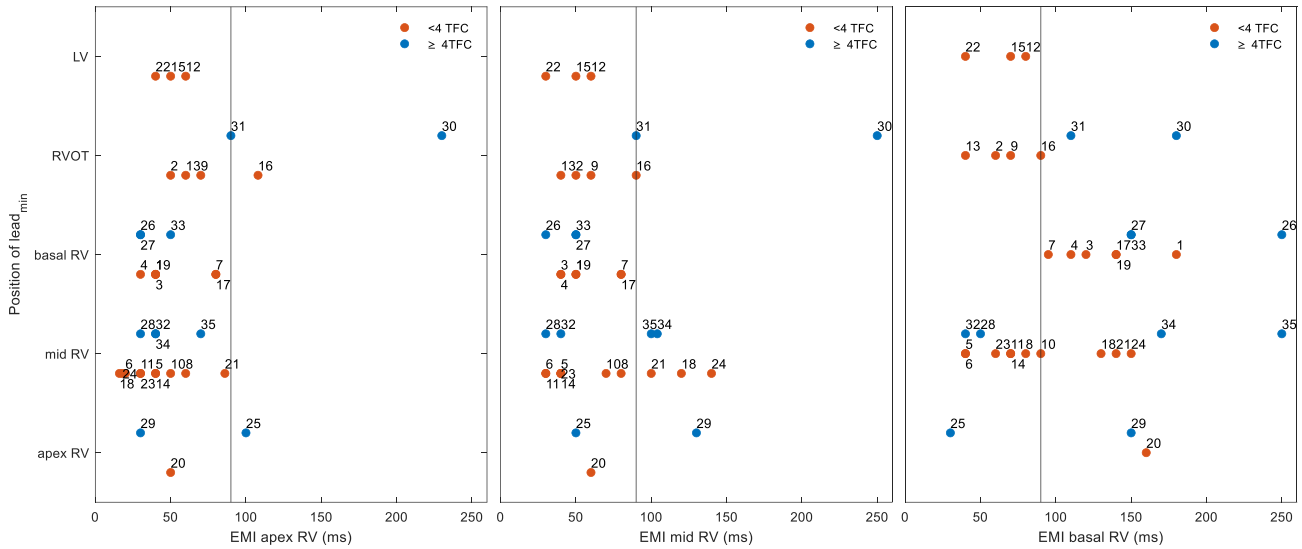

Figure 3: The position of $\overrightarrow{\text{lead}_{min}}$ in relation to the EMI of RV_{apex} (left panel), RV_{mid} (middle panel) and RV_{basal} (right panel). Each dot represents a subject which is labeled by the same number in each plot. An orange dot represents a pathogenic mutation carrier (<4 TFC) and a blue dot represents a definite ACM patient (≥ 4 TFC). The horizontal line in all figures indicates the pathological limit of EMI > 90 ms.

3. Results

The relation between the direction of $\overrightarrow{lead_{min}}$ and EMI is presented in Figure 3. For pathogenic mutation carriers, $\overrightarrow{Lead_{min}}$ directing towards RV_{basal} (9/35) was related to an EMI > 90 ms in RV_{basal}. All patients (5/35) showing $\overrightarrow{lead_{min}}$ in RV_{mid} and a prolonged EMI in RV_{basal} showed also a prolonged EMI in RV_{mid}. $\overrightarrow{Lead_{min}}$ directing towards RV_{apex} resulted for only one patient in a prolonged EMI of RV_{apex}, for one patient in RV_{basal} and for one patient in RV_{mid} and RV_{basal}. A position of $Lead_{min}$ towards the RVOT resulted for three cases in a prolonged EMI in all segments. $\overrightarrow{Lead_{min}}$ directing towards the LV was not related to an EMI > 90ms.

Pathogenic mutation carriers showing no prolonged EMI in any segment (n = 15), showed $\overrightarrow{Lead_{min}}$ the most towards RV_{mid} (9/15), followed by the RVOT (3/15) and the LV (3/15). Remarkably, no control subject showed a position of $\overrightarrow{Lead_{min}}$ towards RV_{basal}. In most cases, $\overrightarrow{Lead_{min}}$ was directed towards RV_{mid} (15/25), followed by the RV_{apex} (7/25), the RVOT (3/25) and the LV (1/25). Mean, 25th and 75th percentiles of the EMI of healthy controls in the RV_{apex} were 0.03 [0.02 0.04], 0.03 [0.02 0.05] in RV_{mid} and 0.05 [0.02 0.07] in RV_{basal}.

4. Discussion

In this study we analyzed electromechanical uncoupling in subclinical pathogenic mutation carriers and ACM patients by relating BSPM to echocardiographic deformation imaging observations. All patients (9/35) showing $\overrightarrow{Lead_{min}}$ directing towards RV_{basal} showed a prolonged EMI in RV_{basal} suggesting a relationship in the electro-mechanical uncoupling of RV_{basal}. Moreover, patients showing $\overrightarrow{lead_{min}}$ in RV_{mid} and a prolonged EMI in RV_{basal} showed also a prolonged EMI in RV_{mid}, indicating that disease involvement of RV_{mid} and RV_{basal} may result in $\overrightarrow{lead_{min}}$ directing towards RV_{mid}.

To the best of our knowledge, there has not been any report on the relationship between echocardiographic deformation imaging and BSPM to describe the electro-mechanical uncoupling in pathogenic PKP2 mutation carriers. An EMI > 90 ms in the subtricuspid region is known to be a marker of disease onset in asymptomatic mutation carriers.[4] This was also observed in this study as the segment RV_{basal} showed a prolonged EMI in most cases (20/35) compared to 9/35 in RV_{mid} and 4/35 in RV_{apex}. Moreover, we observed a relation of $\overrightarrow{lead_{min}}$ pointing towards RV_{basal} and an increased EMI in this area, thereby suggesting the existence of an electro-mechanical relationship in RV_{basal}. $\overrightarrow{Lead_{min}}$ directing towards RV_{mid} and a prolonged EMI in RV_{basal} and RV_{mid} may also indicate an electro-mechanical relationship in this segment, it is however not distinctive as $\overrightarrow{lead_{min}}$ directed also to RV_{mid} in healthy controls (15/25). The same holds for $\overrightarrow{lead_{min}}$ directing towards RV_{apex} and the RVOT. Although all patients with $\overrightarrow{lead_{min}}$ directing towards RV_{apex} had a prolonged EMI in some segment, $\overrightarrow{lead_{min}}$ was

also often directed towards RV_{apex} in the control group (7/25). $\overrightarrow{Lead_{min}}$ directing towards the RVOT resulted for three cases in a prolonged EMI in all segments, suggesting that $\overrightarrow{lead_{min}}$ directing towards the RVOT might be related to a more advanced disease state. However, also three asymptomatic ACM patients and 3/15 healthy controls showed $\overrightarrow{lead_{min}}$ directing towards the RVOT.

Remarkably, $\overrightarrow{lead_{min}}$ was not directed towards RV_{basal} in any healthy control. Therefore, a clear relationship seems to exist between $\overrightarrow{lead_{min}}$ directing towards RV_{basal} and a prolonged EMI in the basal segment. However, $\overrightarrow{Lead_{min}}$ directing towards RV_{basal} was only observed in 9/35 patients. This observation should therefore be further investigated in a larger study population. Another limitation is that the BSPM and echocardiographic deformation imaging control population were different individuals. Although the BSPM control population had no structural abnormalities on MRI, it might be better to create a control population undergoing both measurements to enable a more equal comparison.

Another limitation is the annotation of QRS onset during speckle tracking analysis and thereby the computation of the EMI as it is limited by the low frame rate (70-110 frames/second) of echocardiographic deformation imaging. Time related deformation parameters are therefore error sensitive and in comparison to BSPM parameters, computed with the high sample frequency of 1000 Hz, should be done with caution. Therefore, a strain related parameter or a combination of both strain and time seems more appropriate. Moreover, the relationship towards other segments remains unclear so a more distinctive parameter should be found to study the electromechanical relationship in PKP2 pathogenic mutation carriers.

The comparison between heart segments by BSPM and echocardiographic deformation imaging in this study is new. In a previous study, a PKP2 mouse model showed the existence of a subcellular inter-relationship caused by a cross talk between desmosomal and sodium channel proteins indicating that modifications in desmosomal proteins can affect the sodium current in the absence of structural heart disease.[4] This suggests the role of a purely electrical mechanism in the early onset of ARVC before the presence of structural changes. However, until now, we were not able to detect this by the 12-lead ECG as it might not be sensitive enough to detect these subtle changes. Echocardiographic deformation imaging was the only modality capable in detecting subtle functional abnormalities in the absence of electrical or structural abnormalities by ECG and conventional imaging.[4]

It is expected that a BSPM parameter can be identified in PKP2 pathogenic mutation carriers showing no clinical symptoms or abnormal deformation patterns since electrical changes are likely to precede structural abnormalities. As the population consisted of a relatively large part of pathogenic mutation carriers showing no prolonged EMI in any segment (15/35) it is expected that some of these patients might show electrical abnormalities by BSPM. Future research will therefore focus on the identification of BSPM parameters other than $\overrightarrow{lead_{min}}$ and a combination will be made of both time and strain related deformation parameters to further investigate the electromechanical relationship in PKP2 pathogenic mutation carriers. Moreover, intra-individual analysis will be performed as ACM is known to be a heterogenous disease. In addition, also analysis of the LV will be included since recently also LV involvement has been described in literature.[1]

5. Conclusion

With this study, the first step towards relating both electrical and mechanical changes in ACM pathogenic mutation carriers is made. $\overrightarrow{Lead_{min}}$ directing towards RV_{basal} and a prolonged EMI in this segment suggests the existence of an electro-mechanical relationship in RV_{basal}. Future research will focus on studying other deformation and BSPM parameters to further investigate the electromechanical uncoupling in both pathogenic mutation carriers and ARVC patients. In this way, we will hopefully be able to improve accurate predication and risk stratification of ACM pathogenic mutation carriers in the future.

6. References

[1]C. Miles *et al*., "Sudden Death and Left Ventricular Involvement in Arrhythmogenic Cardiomyopathy," *Circulation*, Apr. 2019.

[2]S. Costa, M. Cerrone, A. M. Saguner, C. Brunckhorst, M. Delmar, and F. Duru, "Arrhythmogenic cardiomyopathy: An in-depth look at molecular mechanisms and clinical correlates," *Trends Cardiovasc. Med.*, Jul. 2020.

[3]E. Gandjbakhch, A. Redheuil, F. Pousset, P. Charron, and R. Frank, "Clinical Diagnosis, Imaging, and Genetics of Arrhythmogenic Right Ventricular Cardiomyopathy/Dysplasia: JACC State-of-the-Art Review," *Journal of the American College of Cardiology*, 14-Aug-2018.

[4]T. P. Mast *et al.*, "The Prognostic Value of Right Ventricular Deformation Imaging in Early Arrhythmogenic Right Ventricular Cardiomyopathy," *JACC Cardiovasc. Imaging*, Mar. 2019.

[5]H. Tandri *et al.*, "Prolonged RV endocardial activation duration: A novel marker of arrhythmogenic right ventricular dysplasia/cardiomyopathy," *Hear. Rhythm*, 2009.

[6]V. L. Aengevaeren *et al.*, "Cardiac Biomarker Kinetics and Their Association With Magnetic Resonance Measures of Cardiomyocyte Integrity Following a Marathon Run: Implications for Postexercise Biomarker Testing," *J. Am. Heart Assoc.*.

Address for correspondence:
Manon Kloosterman
Heidelberglaan 100, 3584 CX Utrecht, the Netherlands
manon.kloosterman@live.com